Reconfigurable Dipolar Spin-Wave Coupling in a Bilateral Yttrium Iron Garnet Structure

A.A. Grachev[1,*] S.E. Sheshukova,[1] M.P. Kostylev,[2] S.A. Nikitov,[1,3] and A.V. Sadovnikov[1,†]

[1] *Laboratory "Magnetic Metamaterials", Saratov State University, Saratov 410012, Russia*

[2] *Department of Physics and Astrophysics M013, University of Western Australia, Crawley 6009, Australia*

[3] *Kotel'nikov Institute of Radioengineering and Electronics, RAS, Moscow 125009, Russia*

(Received 2 April 2021; revised 8 August 2022; accepted 13 February 2023; published 30 May 2023)

We report on the coupling of spin waves propagating as guided modes of yttrium iron garnet stripes. Three stripes are placed parallel to each other and separated by gaps that are small enough to provide nearest-neighbor coupling. We term this geometry "bilateral stripes." The origin of the coupling is the long-ranging dynamic, stray (dipole) field of the precessing magnetization vector. We propose controlling characteristics of this coupling through variation of the static magnetization angle with respect to the main axes of the geometry. We verified the functionality of the proposed magnonic coupler with a micromagnetic simulation of spin-wave propagation along the bilateral stripes. The micromagnetic numerical simulation yielded spectra of transmission of spin waves through the device prototype. Analysis of those spectra revealed that the bilateral stripes can be used as a functional unit in planar magnonic networks—they can be employed as a directional coupler, spin-wave multiplexer, or microwave power divider. Using Brillouin light scattering spectroscopy, we experimentally demonstrated spin-wave transport along the bilateral stripes. We were able to control the spin-wave routing between the stripes ("magnetic channels") by varying the angle of the bias magnetic field.

DOI: 10.1103/PhysRevApplied.19.054089

I. INTRODUCTION

The study of spin-wave phenomena in nanoscale magnetic structures [1–5] is of fundamental interest for understanding the processes of wave propagation and transformation in media with reduced dimension (one-dimensional and two-dimensional) and distributed inhomogeneities—in periodic, modulated, and discrete media [6–15]. The quasiparticles associated with the eigenexcitations in magnetic materials that are known as spin waves are magnons [7,16]. Magnons can be used as information carriers in magnonic circuits. The development of spintronics and magnonics has led to the creation of micro- and nanostructures that are promising candidates for components of magnetic memory and logic in devices with ultralow energy consumption and especially in neuromorphic computing [17,18]. Using spin waves opens up the possibility of constructing complex two- and three-dimensional networks [5,9,19–21] and allows control of nonlinear phenomena [5,22] and supplementing the computing units of memory cells [23].

In particular, collective spin-wave modes on spatially periodic arrays of magnetic nanostripes were investigated [24]. The collective character of the dynamics originates from coupling of the magnetization precession in individual stripes through a dynamic stray (dipole) magnetic field that the precession creates. The field is strongly affected by the confined geometry of the stripe and dictates a quantization condition for the spin-wave modes on both individual and dipole-coupled arrays of stripes [24,25].

Importantly, it has been demonstrated experimentally that coupling between spin waves (or spin-wave beams) can be used to manipulate magnon transport [26–29]. Based on this phenomenon, multiple components of magnonic networks can be built, for instance, a dual-channel directional coupler [3,28,30], spin-wave power splitter [31,32], and tunable frequency-selective all-magnonic unit. Furthermore, coupled spin waves can be used to study the nonlinear spin-wave dynamics [28]. For all these applications, the ability to manipulate the coupling is important. For instance, the magnon transport can be controlled by applying an electric field to multiferroic structures [11,33] and with laser heating [34,35].

An alternative mechanism of spin-wave switching can be implemented by varying the angle at which a static magnetic field is applied to a spin-wave guiding structure [22].

Here we report on coupling of spin waves propagating as guided modes of yttrium iron garnet (YIG) stripes. Three

*Andrew.A.Grachev@gmail.com

†SadovnikovAV@gmail.com

stripes are placed parallel to each other and separated by air gaps that are small enough to provide strong nearest-neighbor coupling. We will term this geometry "bilateral stripes." The origin of the coupling is the long-ranging dynamic stray (dipole) field of the precessing magnetization vector. We propose controlling characteristics of this coupling by varying the angle of the static magnetization with respect to the main axes of the geometry. We verified the functionality of the proposed magnonic coupler with a micromagnetic simulation of spin-wave propagation along the bilateral stripes. The micromagnetic numerical simulation yielded spectra of transmission of spin waves through the device prototype. Analysis of those spectra revealed that the bilateral stripes can be used as a functional unit in planar magnonic networks—they can be utilized as a directional coupler, spin-wave multiplexer, or microwave power divider. Using Brillouin light scattering (BLS) spectroscopy, we experimentally demonstrated spin-wave transport along the bilateral stripes. We were able to control the spin-wave routing between the stripes by varying the bias angle of the magnetic field.

II. SAMPLE FABRICATION

A sketch of the investigated bilateral magnonic structure is shown in Fig. 1(a). The structure consists of three parallel magnetic stripes S_1, S_2, and S_3. The stripes represent three spin-wave channels. The bilateral stripes were fabricated from a YIG [$Y_3Fe_5O_{12}$ (111)] film, $t = 10$ μm thick, grown with high-temperature liquid-phase epitaxy on a 500-μm-thick gallium gadolinium garnet [$Gd_3Ga_5O_{12}$ (111)] substrate. The setup exploits a locally resolved laser ablation technique. A fiber neodymium-doped yttrium aluminum garnet laser with a high-precision two-dimensional galvanometric Cambridge Technology 6240H scanning module was employed in a pulsed regime with a pulse power of 50 J and a pulse duration of 10 ns in order to ablate the target material. The saturation magnetization of the fabricated YIG film was measured independently. We found that $M_0 = 1.39 \times 10^5$ A/m.

The width of each magnetic stripe was $w = 500$ μm. The stripe edge-to-edge separation $d = 40$ μm. The length of the stripes (in the y direction) was 6 mm for S_1 and S_3, and 8 mm for S_2. Spin waves in the structure were excited using a microstrip antenna with a thickness of 1 μm (in the z direction) and a width of 30 μm (in the y direction). In order to excite spin waves, we applied a microwave current to the input antenna. The current was in the form of a train of 100-ns-long microwave pulses with repetition period of 2 μs. We chose the pulse regime in order to avoid heating of S_2 in the vicinity of the shortened microwave antenna.

The structure was magnetized by an external bias magnetic field, $B_0 = 120$ mT. The angle φ between the magnetic field and the x–y plane was varied. Thus, for $\varphi = 90°$ the surface magnetostatic spin waves (MSSWs, $k \perp B_0$)

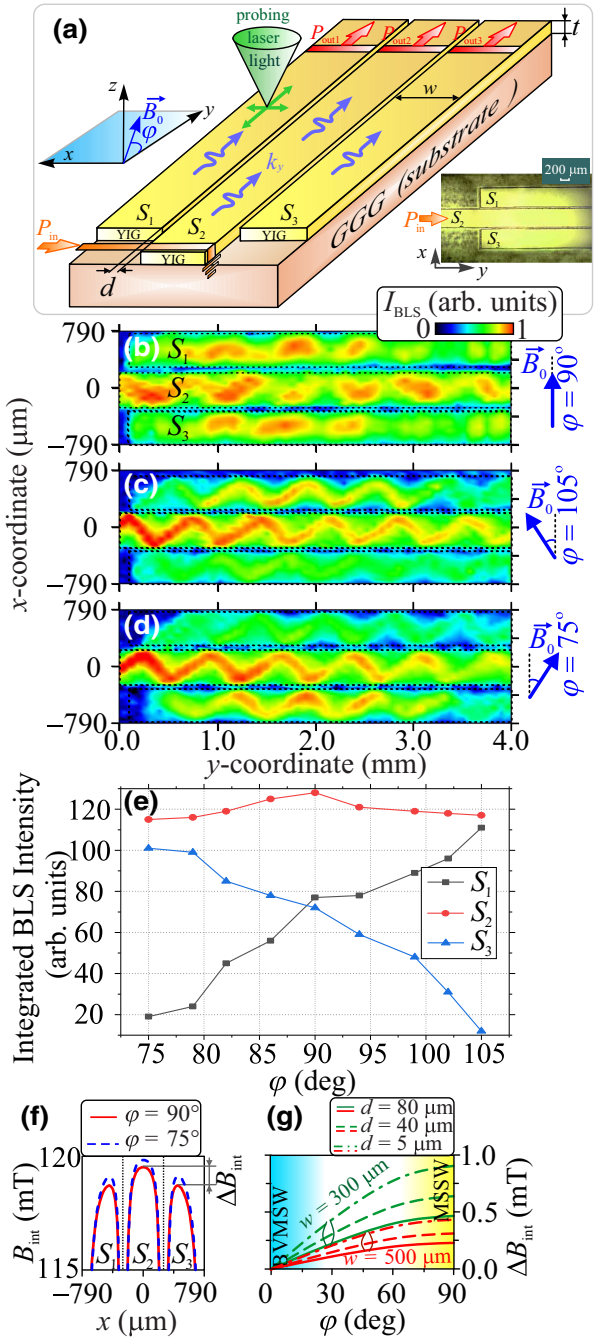

FIG. 1. (a) Sketch of the bilateral magnonic structure. The red stripes in the sketch are microstrip antennas. An input microwave signal denoted by P_{in} is fed into an input antenna. The output antennas are able to pick up the signal carried by traveling spin waves and convert it back into microwave power P_{out}. (b)–(d) Spatial maps of the intensity of the spin wave, measured using Brillouin light scattering spectroscopy for various bias angles φ (at frequency $f_{MSSW} = 5.25$ GHz). (e) Integrated magnetostatic wave (MSSW) Brillouin light scattering intensity as a function of φ for S_1 (gray squares), S_2 (red circles), S_3 (blue triangles). (f) Profiles of the internal magnetic field of the lateral structure for $\varphi = 90°$ (red solid curves) and $\varphi = 75°$ (blue dashed curves). (g) ΔB_{int} as a function of the bias field angle φ for different width and gaps values.

[36,37] are efficiently excited in S_2 and for $\varphi = 0°$ the backward-volume magnetostatic waves (BVMSWs, $k \parallel B_0$) are excited. It should be noted that we consider the propagation of spin waves in the longitudinal direction (along the stripe) and the wave vector component we operate with below is the vector component along the wave propagation direction [the y direction in Fig. 1(a)]. Due to the long-ranging character of the dynamic stray field in the stripe geometry, S_2 can interchange spin-wave energy with S_1 and S_3 in a periodic manner [26].

III. BRILLOUIN LIGHT SCATTERING SPECTROSCOPY STUDY OF THE SPIN-WAVE ROUTING IN BILATERAL STRIPES

The experimental study of the dynamics of the MSSW was carried out using Brillouin light scattering spectroscopy of magnetic materials in the backscattering configuration as shown in our previous works [26–29]. The Brillouin light scattering spectroscopy experiments were performed using a Sandercock (3+3)-pass tandem Fabry-Perot interferometer. A beam of 50 mW of p-polarized green light from a single-mode solid-state Excelsior laser (EXLSR-532-50-CDRH) was focused on the sample surface using a Nikkor lens of numerical aperture 1.2 and focal length 50 mm. The scattered light was collected by the same objective. The technique of signal suppression from elastically scattered and surface phonon-scattered light was used to separate the contribution of magnons to the signal from inelastically scattered light. Spatial maps of spin-wave intensity I_{BLS} were obtained by scanning with the probing light spot in the x and y direction with a resolution of 25 μm and then integrating over the pulse repetition period.

The intensity of the scattered light scales as the spin-wave intensity. The Brillouin light scattering intensity maps are shown for different angles φ in Figs. 1(b)–1(d) for a frequency of $f_{\mathrm{MSSW}} = 5.25$ GHz. It can be seen that when the angle φ changes, a transformation of the spatial intensity distribution takes place for S_1 and S_3. In particular, a decrease in I_{BLS} for S_3 ($\varphi = 105°$ [see Fig. 1(c)]) and S_1 ($\varphi = 75°$ [see Fig. 1(d)]) is visible. One more feature of the intensity maps is an S-shaped variation of the intensity along the individual stripes. This intensity structure was originally seen in [38] and termed "snake structure." It was explained as interference of the first and second width modes of individual stripes that exists at the same frequency. From Figs. 1(b)–1(d) one can see that the interference becomes more pronounced if the bias angle deviates from 90°. It may be explained by an increase in the efficiency of excitation of the antisymmetric second width mode, when the symmetry of the system is reduced by applying the bias field at an angle to the x axis. Figure 1(e) demonstrates how the spatial distribution of the Brillouin light scattering intensity changes when the bias angle φ is varied. The distributions are displayed for a cross section $y = 3$ mm. One can see almost the same intensity for S_1 and S_2 for $\varphi = 90°$. Reducing the angle φ to 75° or increasing ir to 105° results in a redistribution of the spin-wave intensity in the side stripes.

We would like to emphasize that in contrast to previous work [29], where spin-wave excitations are controlled by using mechanical deformations locally on a single stripe, we experimentally demonstrated our concept, based on controlling the "global" external magnetic field that is the same for all three stripes. One possible way to change the direction of the global field is by adding a smaller field in the direction along the stripes that is perpendicular to the main field, such that the vector sum of the two fields represents a vector with a desired angle. This can be achieved by introducing miniature Helmholtz coils to the design.

IV. NUMERICAL SIMULATION AND DISCUSSION

A. Micromagnetic simulation of spin-wave propagation in bilateral magnonic stripes

In order to confirm the experimentally observed control of the distribution of the intensity of the spin-wave signal through a change in the bias angle, a numerical simulation was carried out based on the solution of the Landau-Lifshitz-Gilbert equation [39]

$$\frac{\partial \mathbf{M}}{\partial t} = \gamma[\mathbf{B}_{\mathrm{eff}} \times \mathbf{M}] + \frac{\alpha}{M_0}\left[\mathbf{M} \times \frac{\partial \mathbf{M}}{\partial t}\right], \qquad (1)$$

where $\mathbf{M}$ is the magnetization vector, $\gamma = 28$ GHz/T is the gyromagnetic ratio for the YIG film, $\alpha = 10^{-5}$ is the Gilbert damping parameter, and $\mathbf{B}_{\mathrm{eff}} = \mathbf{B}_0 + \mathbf{B}_{\mathrm{demag}} + \mathbf{B}_{\mathrm{ex}} + \mathbf{B}_a$ is the effective magnetic field, in which $\mathbf{B}_0$ is the external magnetic field, $\mathbf{B}_{\mathrm{demag}}$ denotes the demagnetizing field, $\mathbf{B}_{\mathrm{ex}}$ denotes the exchange field, and $\mathbf{B}_a$ is the anisotropy field.

The finite width of the magnetic stripes in the x direction leads to an inhomogeneous distribution of the internal (static) magnetic field. First, we calculate profiles of the internal magnetic field along the x direction of the considered structure. We do this because we expect that the nonuniformity of the internal magnetic field profile may affect the interstripe dynamic coupling. We find that the internal magnetic field has an asymmetric profile across S_1 and S_3 [see Fig. 1(f)] with the respect to the center of each stripe. An angle variation of [see the blue dashed curves in Fig. 1(f)] leads to an increase in ΔB_{int}, which in turn will shift the spin-wave spectrum. Figure 1(g) shows the magnitude of the internal magnetic fields for the stripes as a function of φ. It is seen that the magnitude changes with increasing bias angle. In order to quantify the effect with a single parameter, we introduce a parameter $\Delta B_{\mathrm{int}} = B_{\mathrm{int2}} - B_{\mathrm{int1,3}}$. This represents the difference in the internal fields of S_2 and S_1 or S_3 [see Fig. 1(f)].

An increase in the bias angle φ leads to an increase of ΔB_{int}, as shown in Fig. 1(g). In our simulation, we find that the profile of the static magnetic field across the structure width (in the x direction) depends on the magnitude of the saturation magnetization for the magnetic material and the sizes of the channels. For $\varphi = 0°$, the demagnetizing field is practically vanishing, and therefore $\Delta B_{\text{int}} = 0$ as expected. Conversely, ΔB_{int} is significant for $\varphi = 90°$, and varies strongly with the edge-to-edge stripe separation. For instance, we found that for $w = 500$ μm, ΔB_{int} increases by about twice when the separation changes from 80 μm to 5 μm. This is important, because the change in the separation results in a noticeable change in the magnitude of the coupling between the spin waves propagating in adjacent stripes [26].

The left column of Fig. 2 shows the spin-wave intensity distribution $I(x,y) = m_x^2 + m_z^2$ in the case of MSSW excitation at $f_{\text{MSSW}} = 5.25$ GHz. As stated above, experimentally observed Brillouin light scattering intensity is known to scale as spin-wave intensity. Therefore, the experimentally measured Brillouin light scattering intensity is a good proxy to the spin-wave intensity. These data are shown for two bias angles φ. First of all, one can see good qualitative agreement between the experiment [Figs. 1(b)–1(d)] and the simulation. In particular, the simulation demonstrates the transfer of power from S_2 to S_1 and S_3 with efficiency similar to the experiment. One also notices the same snake-like structure of intensity as in the experiment, and that the structure becomes more pronounced when the direction of the bias field is tilted with respect to the x axis. To carry out quantitative estimates, we introduce the coupling length. In a simpler case of two lateral ferrite waveguides, the term "coupling length" is defined as the distance over which the energy of a spin wave is completely transferred from one waveguide to another. Within the bilateral system, the coupling length L_{c21} can be entered as the distance at which the energy of the spin wave is transferred from S_2 to S_1 and S_3. It should be said that a complete transfer of spin-wave power is possible only in the case of BVMSW, since in this case the internal magnetic fields are equal in all stripes. In the case of MSSW, only a partial transfer of spin-wave power to the side stripes is observed. In addition, one can see that when the applied field tilts towards the x axis, transformation of the spatial intensity distribution for the side stripes S_1 and S_3 takes place in the simulation. The transformation is very similar to that seen in the experimental Brillouin light scattering spectroscopy maps from Figs. 1(b)–(d). In particular, one observes a decrease in the Brillouin light scattering intensity for S_3. A similar transformation is observed for BVMSW [Figs. 2(c) and 2(d)] for $f_{\text{BMSW}} = 5.23$ GHz. Note that in the case of BVMSW, this effect is more pronounced. However, in the case of micromagnetic modeling of spatial intensity maps for MSSW, the effect is difficult to distinguish due to the color scale. Figures 2(e) and 2(f) respectively show the

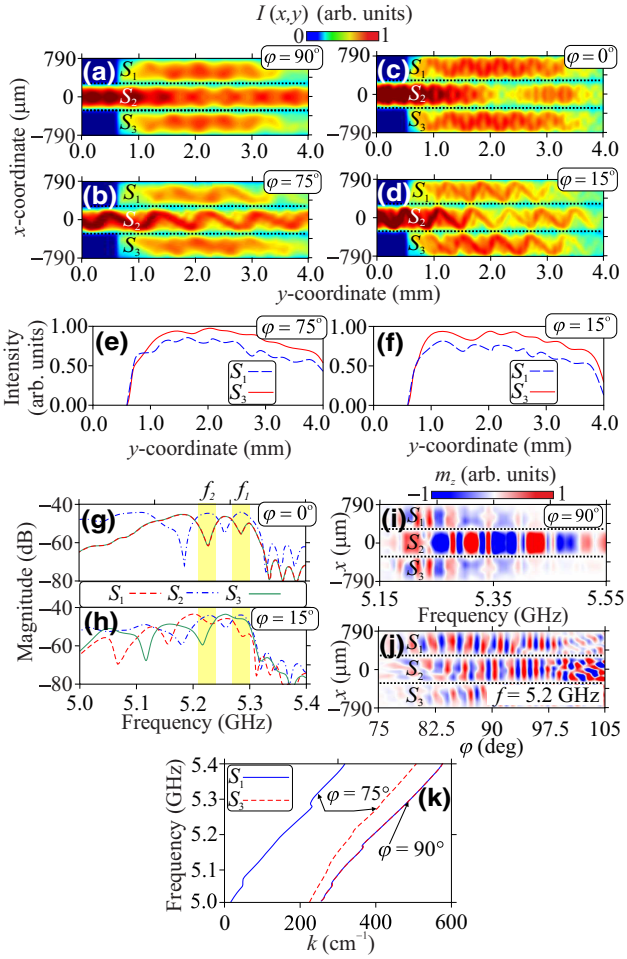

FIG. 2. Simulated spin-wave intensity maps for different bias angles for MSSW (at frequency $f_{\text{MSSW}} = 5.25$ GHz) (a),(b) and BVMSW (at frequency $f_{\text{BMSW}} = 5.23$ GHz) (c),(d). The intensity distributions of the MSSW for $\varphi = 75°$ (e) and of the BVMSW for $\varphi = 15°$ (f) for the S_1 and S_3 stripes. Simulated spectra of power density of the output signal $P_{1,2,3}(f)$ in the case of BVMSW propagation, when the bias angle $\varphi = 0°$ (g) and $\varphi = 15°$ (h). Simulated spatial map of the components of dynamic magnetization m_z as a function of frequency for $\varphi = 90°$ (i) and as a function of the angle φ for a fixed frequency, the value of which is shown in (j). (k) Simulated frequency dependence of the effective wave number.

intensity distributions for the MSSW for $\varphi = 75°$ and the BVMSW for $\varphi = 15°$ in the centers of S_1 and S_3. An asymmetric propagation is seen in this case that is accompanied by a decrease in the spin-wave power in S_1, and a slight change in the spin-wave coupling length in S_1.

This good agreement between experiment and simulation allows us to use simulation results in order to gain more detail of the experimentally observed effects. First, we calculate the spectral power density for the output signal $P_{1,2,3}(f)$ and a cross section $y = 3.0$ mm. The power densities are obtained by integrating across the widths of individual stripes (i.e., in the x direction). For

this, the input signal was set to $b_z(t) = b_0\mathrm{sinc}(2\pi f_c t)$, frequency $f_c = 7$ GHz, $b_0 = 0.01$ mT. Then the value of the dynamic magnetization $m_z(x, y, t)$ in the region of the output section $P_{1,2,3}$ was recorded in steps of $\Delta t = 75$ fs during a time interval of $T = 500$ ns. Finally, we employ a two-dimensional fast Fourier transform , in order to generate a frequency dependence of the dynamic magnetization at the output $P_{1,2,3}(f)$ of the bilateral stripes. We do this as a function of frequency and for the case of BVMSW propagation [see Figs. 2(g) and 2(h)]. One can see that when the angle of the bias field changes, redistribution of power is observed, as well as a break of symmetry in the spectra for S_1 and S_3.

Figure 2(i) illustrates the frequency dependence of the efficiency of the signal transfer between the stripes. The simulation is done for $\varphi = 90°$. We choose the z component of dynamic magnetization (m_z) as the quantify characterizing the signal. It can be seen that in the frequency range from 5.17 GHz to 5.4 GHz, a part of the energy of the spin wave is transferred from S_2 to S_1 and S_3. At $f > 5.4$ GHz, the power of the spin wave is mainly localized in the central stripe S_2. Figure 2(j) shows the effect of the sign of φ on m_z (spin-wave phase) for the same cross section $y = 3.0$ mm at a fixed frequency of 5.17 GHz. With a gradual change in the magnitude of the angle, a change in the magnitude and sign of m_z is observed.

In order to better understand the break in symmetry associated with the application of the bias field at an angle with respect to the x symmetry axis, we extract effective dispersion laws for spin waves in the individual stripes of the bilateral structure. Figure 2(k) shows the effective wave numbers for the frequency range of excitation of MSSW. The wave number was extracted from the raw simulation data using the formula $k_{\mathrm{eff}}(f) = (\zeta(f) - \zeta_S(f))/L$, where $\zeta(f)$ is the phase shift of the spin wave along the length L between the region of the input and output antennas and $\zeta_S(f)$ is the initial phase on the excitation source of spin waves. From the figure, one can see that for the highest-symmetry case $\varphi = 90°$, the dispersion characteristics for S_1 [red dashed curve in Fig. 2(k)] and S_3 [blue solid curve in Fig. 2(k)] are the same. When the symmetry is broken by applying the field at an angle of 15° to the x axis ($\varphi = 75°$), the degeneracy in the frequencies for S_1 and S_3 is lifted. This occurs due to changes to the phase shift $\zeta(f)$.

In the case of dipolar propagation of spin waves in the bilateral structure considered, the frequency increase for $\varphi = 75°$ is primarily associated with an increase in the magnitude of the internal magnetic field in the YIG stripes. When considering the static problem, we see an increase in B_{int} in the centers of the waveguides when passing from the case of 90° to 75°. If dynamic demagnetization is not taken into account, changing the bias angle will increase the frequency of the beginning of the spectrum and shift the dispersion curve of each mode to the high-frequency region.

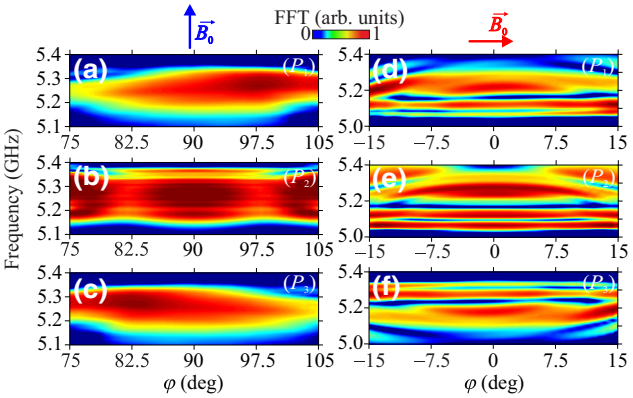

FIG. 3. Spectral power density maps for each magnonic stripe S_1 (a),(d), S_2 (b),(e), S_3 (c),(f) as a function of bias angles φ. (a)–(c) MSSW; (d)–(f) BVMSW.

Similarly, the degeneracy in spectral power densities is also lifted, by applying the field at an angle. Further evidence of the importance of the system's symmetry that may be broken by applying the bias field at an angle is displayed in Fig. 3. This figure displays spectral power density maps for each magnonic stripe S_1 [Figs. 3(a) and 3(d)], S_2 [Figs. 3(b) and 3(e)], S_3 [Figs. 3(c) and 3(f)] as a function of the bias field angle φ in the case of MSSW [Figs. 3(a)–3(c)] and BVMSW [Figs. 3(d)–3(f)]. One can see a pronounced antisymmetry of the effects of φ for S_1 and S_3. One can also clearly see that in the case of MSSWs a decrease in the width of the frequency spectrum and a decrease in power of signals at the output ports of the side stripes are observed with tilting the bias field away from the x symmetry axis. The trend is less pronounced for BVMSW.

Next, we considered the case when spin waves are excited in the side magnonic stripe S_3. Figure 4

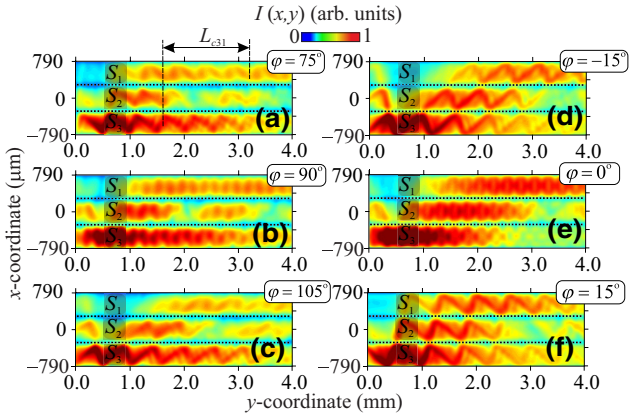

FIG. 4. Calculated intensity maps for various bias field angles. (a)–(c) MSSW (at frequency $f_{\mathrm{MSSW}} = 5.25$ GHz), (d)–(f) BVMSW (at frequency $f_{\mathrm{BVMSW}} = 5.23$ GHz).

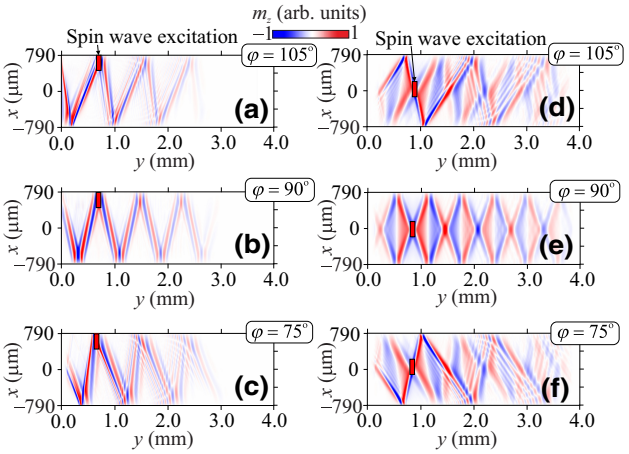

FIG. 5. Spatial maps of the dynamic magnetization component m_z for various bias field angles. $d = 0$, and the initial spin wave is excited by an external source in either the central area (a)–(c) or the side area (d)–(f) by an external source. (at frequency $f_{\mathrm{MSSW}} = 5.25$ GHz).

displays the intensity distribution $I(x,y) = m_x^2 + m_z^2$ for the MSSW configuration (left column) and for different bias field angles φ. One can see that most of the energy of the spin wave remains localized in S_3, due to the unequal internal static magnetic fields in the bilateral stripes [see Fig. 1(f)]. The difference in the internal fields prohibits efficient energy leaking into the adjacent stripe S_2. Conversely, in the case of propagation of BVMSW, complete transfer of the spin-wave power from S_3 to S_1 is possible. The spin-wave power moves in a periodic manner between the stripes. As in the case of excitation of spin waves in S_2, we can introduce the concept of the coupling length L_{c31}. But in this case it will be the distance at which the spin-wave energy is transferred from S_3 to S_1 [see Fig. 4(d)]. In this case, for MSSW [see Figs. 4(a)–4(c)], it becomes difficult to determine L_{c31}, since there is no complete transfer of spin-wave power from S_3. Therefore, we will consider the case of BVMSW [see Figs. 4(d)–4(f)]. It can be seen that the spin-wave energy completely leaves S_3, passing into S_2, and then into S_1 and back. When we change the bias angle φ it leads to a redistribution of the intensity in the bilateral system, as well as a change in L_{c31}. Note that in the case of MSSW, the distance at which the energy of the spin-wave power arrives at S_1 also changes.

A useful way to get a better understanding of the process is by considering the limiting case of $d = 0$. In this case, one is dealing *de facto* with a single waveguide of the triple width. Figure 5 shows spatial maps of m_z for various bias angles for $d = 0$. The initial spin wave is launched into either the central area (a)–(c) or the side area (d)–(f). It can be seen that when the bias angle is varied, the spin-wave propagation front rotates in the direction of rotation of the field vector. In addition, we show in the Supplemental Material [40] that for a waveguide of a triple width, the angles of incidence, reflection, and demagnetizing [41,42] at the edges of the waveguide are not the same when the angle of the external magnetic field with the x axis deviates from 0°. It should be noted that when the spin wave is excited in the lateral part of the waveguide of triple width, a change in the nature of propagation is observed in the simulation, such as a change in the wavelength and the influence of causticlike beam formation, as well as well-pronounced asymmetry of wave propagation [43,44].

We may expect that the picture of the process as revealed in Fig. 5 and the Supplemental Material [40] remains valid for negligibly small separations d, and a slow transition to the dynamics of three uncoupled stripes from this picture will take place with a further increase in d. Thus, the control of the spin-wave propagation through the bilateral structure by varying the angle of the bias field can be explained by a causticlike propagation of the waves and the broken symmetry of reflection of caustic beams from a waveguide edge if the bias field is at an angle to the edge that is not equal to 90°.

Above, we saw that considering reflection of a plane wave from the structure edges provides a useful insight into the origin of the effect of the bias field angle on the spin-wave propagation on the bilateral stripes. Alternatively, one may consider formation of guided modes on this confined geometry and investigate how the mode structure varies with the bias field angle.

B. Eigenmode spectra study of bilateral magnonic stripes by the finite-element method

At the same time, micromagnetic modeling does not allow us to fully assess the spectrum of eigenmodes and, therefore, the effect of changes in the bias angle. To this end, we simulate the spin-wave guided modes in the bilateral stripes using the finite-element method. A two-dimensional model of the lateral structure was constructed and the full system of Maxwell's equations numerically solved. In the case of an arbitrary magnetization angle φ, the magnetic permeability tensor for the YIG stripe can be written as

$$\hat{\mu} = \begin{vmatrix} \mu(f)\sin^2\varphi + \cos^2\varphi & i\mu_a(f)\sin\varphi & (1-\mu(f))\sin\varphi\cos\varphi \\ -i\mu_a(f)\sin\varphi & \mu(f) & i\mu_a(f)\cos\varphi \\ (1-\mu(f))\sin\varphi\cos\varphi & -i\mu_a(f)\cos\varphi & \mu(f)\cos^2\varphi + \sin^2\varphi \end{vmatrix} \quad (2)$$

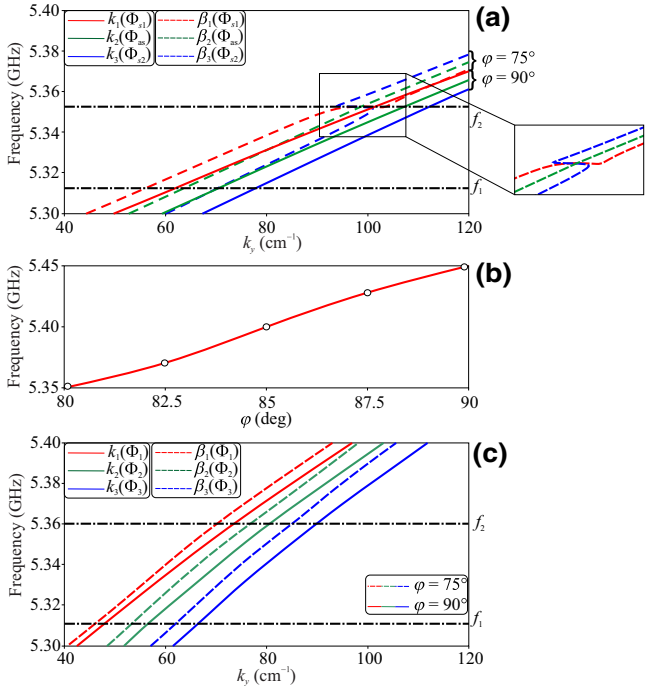

FIG. 6. (a) Dispersion for the eigenmodes of the bilateral structure. Solid lines, $\varphi = 90°$; dashed lines, $\varphi = 75°$. (b) Frequency of crossing of dispersion branches as a function of the bias field angle φ for the bilateral structure. (c) Eigenmode dispersion for the case of a single 1.5-mm-wide magnetic stripe. Solid lines, $\varphi = 90°$; dashed lines, $\varphi = 75°$.

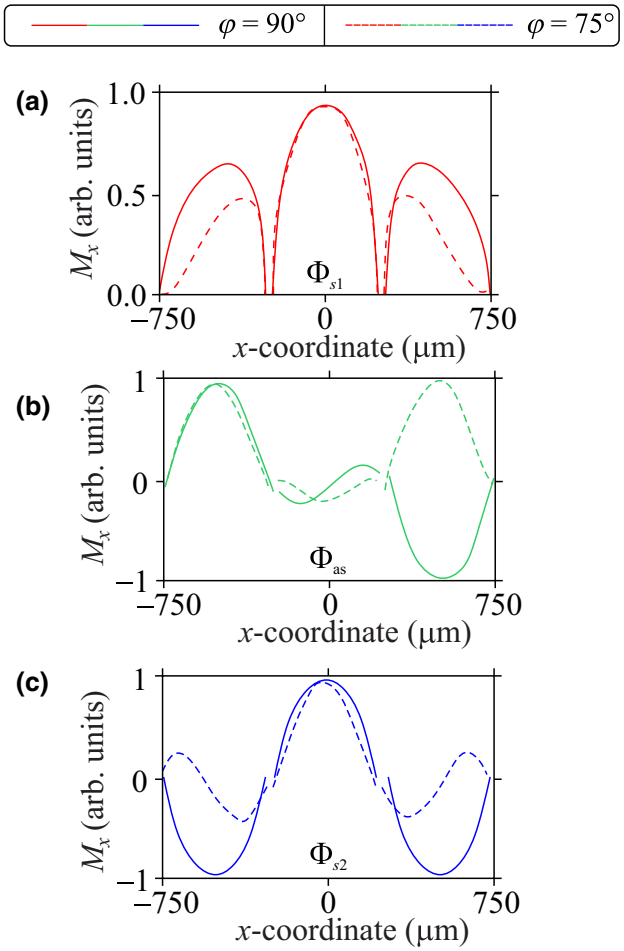

FIG. 7. Eigenmodes of the bilateral magnetic stripes for $\varphi = 90°$ (solid lines) and $\varphi = 75°$ (dashed lines) for frequency f_1.

where $\mu(f) = f_B(f_B + f_M) - f^2/f_B^2 - f^2$, $\mu_a(f) = f_M f / f_B^2 - f^2$, $f_M = \gamma 4\pi M_0 = 4.9$ GHz, $f_B = \gamma B_0 = 3.36$ GHz, and $f_\perp = \sqrt{f_B(f_B + f_M)} = 5.26$ GHz is the frequency of the ferromagnetic resonance in the tangentially magnetized ferrite film. The relative electric permittivity of YIG is $\varepsilon = 14$.

The dipolar coupling of the propagating spin waves in stripes leads to splitting of the spin-wave dispersion into three spin-wave modes with longitudinal wave numbers k_1, k_2, and k_3 [see Fig. 6(a)]. This is similar to standing-wave resonances ($k = 0$) for three dipole-coupled bilateral stripes [24]. The eigenmode spectrum for the three adjacent stripes represents a system of an antisymmetric Φ_{as} [see Fig. 7(b)] and two symmetric (Φ_{s1} [see Fig. 7(a)], Φ_{s2} [see Fig. 7(c)]) modes with the longitudinal wave numbers k_2, k_1, and k_3, respectively. The modes are orthogonal to each other for any given frequency, as expected for the eigenmodes of a waveguide.

From Fig. 6(a) one can see that the mode dispersion in this frequency range is practically linear. Furthermore, for any frequency from the range, the wave numbers of the nearest-neighbor modes differ from each other by $\Delta k = 7.5$ cm^{-1} on average. If several modes are excited simultaneously by a localized source of single frequency, the modes will interfere in space as they propagate down the spin-wave waveguide [38]. The half-period of spatial beat of the modes will amount to $\Delta L_{c21} = \pi/\Delta k = 4$ mm, which is in agreement with the horizontal scale of Figs. 2(c) and 2(d). This allows one to explain switching between the channels as mode interference.

The configuration of dynamic and static demagnetizing fields of the modes determines the relative frequencies of the modes. The profile of the symmetric mode Φ_{s1} (see Fig. S1 in Online Supplemental Material [40]) is the closest to the one for the fundamental mode of a single-stripe waveguide (see Panel B in Fig. 4 from Ref. [45]). Therefore, similarly to the single-stripe case, this mode must possess the highest frequency for any given wave number and $\varphi = 90°$.

To confirm this idea, we computed the spin-wave dispersion and mode profiles for a single-stripe waveguide with a width of 1.5 mm. This width is equal to the total width of the lateral structure. This geometry can be considered as a "parent" one for the bilateral waveguide, as the bilateral waveguide can be formed from the parent structure by adding grooves to the parent geometry. The spin-wave

dispersion for the parent single-stripe waveguide is shown in Fig. 6(c). One can see that the dispersion law is qualitatively similar to the one for the bilateral waveguide. The mode profiles for the parent waveguide are shown in the same Fig. S1 in the Supplemental Material [40] with dashed lines. One can clearly see that the collective guided modes of the bilateral structure strongly resemble those for the single stripe of the triple width. The only exception is the antisymmetric mode Φ_{as} of the bilateral structure for $\varphi = 75^{\circ}$ and f_2. Its single-stripe counterpart is a symmetric mode. A more detailed discussion of eigenmode transformation is given in the Supplemental Material [40]. Here it is important that the idea of the interference of the eigenmodes of the bilateral structure explains well the spin-wave energy transfer between the stripes and its evolution with the angle of the bias field.

This concept of the intensity and phase signal manipulation indicates the possibility of using the proposed bilateral multichannel device as a basic element of signal processing systems based on the principles of neuromorphic [46–51] magnonic logic, such as magnon logic cells based on fuzzy logic elements, neuromorphic multiplexing and demultiplexing systems [17], and space-frequency dividers and couplers [5] of information signals in the microwave and terahertz wavelength range.

V. POTENTIAL APPLICATION

A large number of papers on experimental and numerical demonstration of the use of single [52,53] and lateral ferrite/ferromagnetic microscale waveguides [26,29, 54,55] as directional couplers, phase shifters, and signal dividers have been published. This is because these devices may easily be tuned: their frequency range can be adjusted by changing the external magnetic field, geometric parameters, creating temperature gradients on the surface of microscale waveguides [34,35], as well as creating additional ferroelectric [27], semiconductor [10], and piezoelectric [29,55] loads.

In addition, due to recent progress in technological capabilities, it has become possible to create nanoscale waveguides [4,5,56]. Wang *et al*. [56] numerically investigated three parallel YIG nanostripes in the presence of additional spin-wave damping in the central stripe. A dark mode regime was found in these conditions. This concept allows one to implement a magnonic version of the stimulated Raman adiabatic passage (m-STIRAP) mechanism, which has a high potential for applications by bringing together the wealth of quantum-classical analogy phenomena with the wealth of means to control wave propagation in magnonic systems. In contrast to that work, our structure demonstrates the possibility of controlling the beam of spin waves by changing the angle of the external magnetic field, without the need to increase damping in one of the stripes by adding extra layers to the device geometry. Hence, our geometry is noticeably simpler. In addition, in the present work, we employed the Brillouin light scattering spectroscopy method in order to investigate the spin-wave dynamics of the device. The measurements confirmed the functionality of this device as a spin-wave directional coupler for spintronic application. Furthermore, we have demonstrated that the global control of the magnetic field angle allows control of local characteristics (such as amplitude and phase) of the signal at each of the output ports. For instance, this may be useful in magnonic reservoir computing, whose high potential for applications has recently been demonstrated [57].

VI. CONCLUSION

Using numerical and experimental techniques, we investigated coupling of spin waves propagating as guided modes of YIG stripes. Three stripes are placed parallel to each other and separated by gaps that are small enough to provide efficient nearest-neighbor coupling. The origin of the coupling is the long-ranging dynamic stray (dipole) field of the precessing magnetization vector. We demonstrated control of characteristics of this coupling through variation of the static magnetization angle with respect to the main axes of the geometry.

We verified the functionality of the proposed magnonic coupler with a micromagnetic simulation and propose using this method in order to control a microwave coupler that can be built based on the bilateral stripes. This idea was confirmed experimentally with Brillouin light scattering spectroscopy, which revealed the controlled spin-wave routing between the stripes. The simulation, yielded spectra of transmission of spin waves through the device-prototype. Analysis of those spectra revealed that the bilateral stripes can be used as a functional unit in planar magnonic networks —they can be utilized as a directional coupler, spin-wave multiplexer, or microwave power divider.

ACKNOWLEDGMENTS

This work was supported by the Ministry of Education and Science of the Russian Federation as part of the state assignment (project No. FSRR-2023-0008) and a Research Collaboration Award from the University of Western Australia.

[1] B. Heinz, T. Brächer, M. Schneider, Q. Wang, B. Lägel, A. M. Friedel, D. Breitbach, S. Steinert, T. Meyer, and M. Kewenig, *et al.*, Propagation of spin-wave packets in individual nanosized yttrium iron garnet magnonic conduits, Nano Lett. **20**, 4220 (2020).

[2] P. Che, K. Baumgaertl, A. Kúkol'ová, C. Dubs, and D. Grundler, Efficient wavelength conversion of exchange

magnons below 100 nm by magnetic coplanar waveguides, Nat. Commun. **11**, 1445 (2020).

[3] Q. Wang, P. Pirro, R. Verba, A. Slavin, B. Hillebrands, and A. V. Chumak, Reconfigurable nanoscale spin-wave directional coupler, Sci. Adv. **4**, e1701517 (2018).

[4] Q. Wang, A. Hamadeh, R. Verba, V. Lomakin, M. Mohseni, B. Hillebrands, A. V. Chumak, and P. Pirro, A nonlinear magnonic nano-ring resonator, npj Comput. Mater. **6**, 1 (2020).

[5] Q. Wang, M. Kewenig, M. Schneider, R. Verba, F. Kohl, B. Heinz, M. Geilen, M. Mohseni, B. Lägel, and F. Ciubotaru, *et al.*, A magnonic directional coupler for integrated magnonic half-adders, Nat. Electron. **3**, 765 (2020).

[6] S. Neusser and D. Grundler, Magnonics: Spin waves on the nanoscale, Adv. Mater. **21**, 2927 (2009).

[7] V. V. Kruglyak, S. O. Demokritov, and D. Grundler, Magnonics, J. Phys. D: Appl. Phys. **43**, 264001 (2010).

[8] S. A. Nikitov, D. V. Kalyabin, I. V. Lisenkov, A. Slavin, Y. N. Barabanenkov, S. A. Osokin, A. V. Sadovnikov, E. N. Beginin, M. A. Morozova, and Y. A. Filimonov, *et al.*, Magnonics: A new research area in spintronics and spin wave electronics, Phys.-Usp. **58**, 1002 (2015).

[9] G. Gubbiotti, *Three-Dimensional Magnonics: Layered, Micro-And Nanostructures* (Jenny Stanford Publishing, New York, 2019).

[10] A. V. Sadovnikov, E. N. Beginin, S. E. Sheshukova, Y. P. Sharaevskii, A. I. Stognij, N. N. Novitski, V. K. Sakharov, Y. V. Khivintsev, and S. A. Nikitov, Route toward semiconductor magnonics: Light-induced spin-wave nonreciprocity in a YIG/GaAs structure, Phys. Rev. B **99**, 054424 (2019).

[11] A. V. Sadovnikov, A. A. Grachev, A. A. Serdobintsev, S. E. Sheshukova, S. S. Yankin, and S. A. Nikitov, Magnon straintronics to control spin-wave computation: Strain reconfigurable magnonic-crystal directional coupler, IEEE Magn. Lett. **10**, 1 (2019).

[12] A. Haykal, J. Fischer, W. Akhtar, J.-Y. Chauleau, D. Sando, A. Finco, F. Godel, Y. A. Birkhölzer, C. Carrétéro, and N. Jaouen, *et al.*, Antiferromagnetic textures in $BiFeO_3$ controlled by strain and electric field, Nat. Commun. **11**, 1704 (2020).

[13] Z. Haghshenasfard and M. G. Cottam, Hybrid modes of a cavity photon coupled with multiple magnons in ferromagnetic nanostructures, Phys. Rev. B **101**, 144438 (2020).

[14] B. W. Zingsem, T. Feggeler, A. Terwey, S. Ghaisari, D. Spoddig, D. Faivre, R. Meckenstock, M. Farle, and M. Winklhofer, Biologically encoded magnonics, Nat. Commun. **10**, 4345 (2019).

[15] J. Ding, M. Kostylev, and A. O. Adeyeye, Magnonic Crystal as a Medium with Tunable Disorder on a Periodical Lattice, Phys. Rev. Lett. **107**, 047205 (2011).

[16] A. Barman, G. Gubbiotti, S. Ladak, A. O. Adeyeye, M. Krawczyk, J. Gräfe, C. Adelmann, S. Cotofana, A. Naeemi, V. I. Vasyuchka, and B. Hillebrands, *et al.*, The 2021 magnonics roadmap, J. Phys.: Condens. Matter **33**, 413001 (2021).

[17] T. Brächer and P. Pirro, An analog magnon adder for all-magnonic neurons, J. Appl. Phys. **124**, 152119 (2018).

[18] Á. Papp, W. Porod, and G. Csaba, Nanoscale neural network using non-linear spin-wave interference, Nat. Commun. **12**, 1 (2021).

[19] A. Mahmoud, F. Ciubotaru, F. Vanderveken, A. V. Chumak, S. Hamdioui, C. Adelmann, and S. Cotofana, Introduction to spin wave computing, J. Appl. Phys. **128**, 161101 (2020).

[20] T. Goto, T. Yoshimoto, B. Iwamoto, K. Shimada, C. A. Ross, K. Sekiguchi, A. B. Granovsky, Y. Nakamura, H. Uchida, and M. Inoue, Three port logic gate using forward volume spin wave interference in a thin yttrium iron garnet film, Sci. Rep. **9**, 1 (2019).

[21] E. N. Beginin, A. V. Sadovnikov, A. Y. Sharaevskaya, A. I. Stognij, and S. A. Nikitov, Spin wave steering in three-dimensional magnonic networks, Appl. Phys. Lett. **112**, 122404 (2018).

[22] A. V. Sadovnikov, C. S. Davies, V. V. Kruglyak, D. V. Romanenko, S. V. Grishin, E. N. Beginin, Y. P. Sharaevskii, and S. A. Nikitov, Spin wave propagation in a uniformly biased curved magnonic waveguide, Phys. Rev. B **96**, 060401 (2017).

[23] S. Dutta, S.-C. Chang, N. Kani, D. E. Nikonov, S. Manipatruni, I. A. Young, and A. Naeemi, Non-volatile clocked spin wave interconnect for beyond-CMOS nanomagnet pipelines, Sci. Rep. **5**, 1 (2015).

[24] M. P. Kostylev, A. A. Stashkevich, and N. A. Sergeeva, Collective magnetostatic modes on a one-dimensional array of ferromagnetic stripes, Phys. Rev. B **69**, 064408 (2004).

[25] J. Jorzick, C. Krämer, S. Demokritov, B. Hillebrands, B. Bartenlian, C. Chappert, D. Decanini, F. Rousseaux, E. Cambril, E. So/ndergard, *et al.*, Spin wave quantization in laterally confined magnetic structures, J. Appl. Phys. **89**, 7091 (2001).

[26] A. Sadovnikov, E. Beginin, S. Sheshukova, D. Romanenko, Y. P. Sharaevskii, and S. Nikitov, Directional multimode coupler for planar magnonics: Side-coupled magnetic stripes, Appl. Phys. Lett. **107**, 202405 (2015).

[27] A. Sadovnikov, A. Grachev, E. Beginin, S. Sheshukova, Y. P. Sharaevskii, and S. Nikitov, Voltage-Controlled Spin-Wave Coupling in Adjacent Ferromagnetic-Ferroelectric Heterostructures, Phys. Rev. Appl. **7**, 014013 (2017).

[28] A. Sadovnikov, S. Odintsov, E. Beginin, S. Sheshukova, Y. P. Sharaevskii, and S. Nikitov, Toward nonlinear magnonics: Intensity-dependent spin-wave switching in insulating side-coupled magnetic stripes, Phys. Rev. B **96**, 144428 (2017).

[29] A. Sadovnikov, A. Grachev, S. Sheshukova, Y. P. Sharaevskii, A. Serdobintsev, D. Mitin, and S. Nikitov, Magnon Straintronics: Reconfigurable Spin-Wave Routing in Strain-Controlled Bilateral Magnetic Stripes, Phys. Rev. Lett. **120**, 257203 (2018).

[30] H. Yu, G. Duerr, R. Huber, M. Bahr, T. Schwarze, F. Brandl, and D. Grundler, Omnidirectional spin-wave nanograting coupler, Nat. Commun. **4**, 2702 (2013).

[31] A. V. Sadovnikov, C. S. Davies, S. V. Grishin, V. Kruglyak, D. Romanenko, Y. P. Sharaevskii, and S. Nikitov, Magnonic beam splitter: The building block of parallel magnonic circuitry, Appl. Phys. Lett. **106**, 192406 (2015).

[32] F. Heussner, A. Serga, T. Brächer, B. Hillebrands, and P. Pirro, A switchable spin-wave signal splitter for magnonic networks, Appl. Phys. Lett. **111**, 122401 (2017).

[33] A. V. Sadovnikov, A. A. Grachev, E. N. Beginin, S. E. Sheshukova, Y. P. Sharaevsky, A. A. Serdobintsev, D. M. Mitin, and S. A. Nikitov, Splitting of spin waves in strain reconfigurable magnonic stripe, IEEE Trans. Magn. **53**, 1 (2017).

[34] M. Vogel, A. V. Chumak, E. H. Waller, T. Langner, V. I. Vasyuchka, B. Hillebrands, and G. von Freymann, Optically reconfigurable magnetic materials, Nat. Phys. **11**, 487 (2015).

[35] O. Dzyapko, I. Borisenko, V. Demidov, W. Pernice, and S. Demokritov, Reconfigurable heat-induced spin wave lenses, Appl. Phys. Lett. **109**, 232407 (2016).

[36] R. Damon and J. Eshbach, Magnetostatic modes of a ferromagnet slab, J. Phys. Chem. Solids **19**, 308 (1961).

[37] T. W. O'Keeffe and R. W. Patterson, Magnetostatic surface-wave propagation in finite samples, J. Appl. Phys. **49**, 4886 (1978).

[38] O. Buttner, M. Bauer, C. Mathieu, S. O. Demokritov, B. Hillebrands, P. A. Kolodin, M. P. Kostylev, S. Sure, H. Dotsch, and V. Grimalsky, *et al.*, Mode beating of spin wave beams in ferrimagnetic Lu/sub 2.04/Bi/sub 0.96/Fe/sub 5/O/sub 12/ films, IEEE Trans. Magn. **34**, 1381 (1998).

[39] A. Vansteenkiste, J. Leliaert, M. Dvornik, M. Helsen, F. Garcia-Sanchez, and B. Van Waeyenberge, The design and verification of MuMax3, AIP Adv. **4**, 107133 (2014).

[40] See the Supplemental Material at http://link.aps.org/supplemental/10.1103/PhysRevApplied.19.054089, which shows detailed results of simulating the eigenmode profiles and spin-wave dispersion of the bi-lateral structure.

[41] A. Aharoni, Demagnetizing factors for rectangular ferromagnetic prisms, J. Appl. Phys. **83**, 3432 (1998).

[42] M. Schabes and A. Aharoni, Magnetostatic interaction fields for a three-dimensional array of ferromagnetic cubes, IEEE Trans. Magn. **23**, 3882 (1987).

[43] A. V. Sadovnikov, A. A. Grachev, S. A. Odintsov, S. E. Sheshukova, Y. P. Sharaevskii, and S. A. Nikitov, Spin-wave transport along in-plane magnetized laterally coupled magnonic stripes, IEEE Magn. Lett. **8**, 1 (2017).

[44] C. Davies, A. Francis, A. Sadovnikov, S. Chertopalov, M. Bryan, S. Grishin, D. Allwood, Y. P. Sharaevskii, S. Nikitov, and V. Kruglyak, Towards graded-index magnonics: Steering spin waves in magnonic networks, Phys. Rev. B **92**, 020408 (2015).

[45] M. P. Kostylev, G. Gubbiotti, J.-G. Hu, G. Carlotti, T. Ono, and R. L. Stamps, Dipole-exchange propagating spin-wave modes in metallic ferromagnetic stripes, Phys. Rev. B **76**, 054422 (2007).

[46] J. Torrejon, M. Riou, F. A. Araujo, S. Tsunegi, G. Khalsa, D. Querlioz, P. Bortolotti, V. Cros, K. Yakushiji, and A. Fukushima, *et al.*, Neuromorphic computing with nanoscale spintronic oscillators, Nature **547**, 428 (2017).

[47] D. Marković, N. Leroux, M. Riou, F. A. Araujo, J. Torrejon, D. Querlioz, A. Fukushima, S. Yuasa, J. Trastoy, P. Bortolotti, and J. Grollier, Reservoir computing with the frequency, phase, and amplitude of spin-torque nano-oscillators, Appl. Phys. Lett. **114**, 012409 (2019).

[48] M. Romera, P. Talatchian, S. Tsunegi, F. Abreu Araujo, V. Cros, P. Bortolotti, J. Trastoy, K. Yakushiji, A. Fukushima, and H. Kubota, *et al.*, Vowel recognition with four coupled spin-torque nano-oscillators, Nature **563**, 230 (2018).

[49] L. Chen, S. Urazhdin, Y. Du, and R. Liu, Dynamical Mode Coupling and Coherence in a Spin Hall Nano-oscillator with Perpendicular Magnetic Anisotropy, Phys. Rev. Appl. **11**, 064038 (2019).

[50] W. Yu, J. Lan, and J. Xiao, Magnetic Logic Gate Based on Polarized Spin Waves, Phys. Rev. Appl. **13**, 024055 (2020).

[51] G. Csaba, Á. Papp, and W. Porod, Perspectives of using spin waves for computing and signal processing, Phys. Lett. A **381**, 1471 (2017).

[52] A. B. Ustinov and B. A. Kalinikos, Power-dependent switching of microwave signals in a ferrite-film nonlinear directional coupler, Appl. Phys. Lett. **89**, 172511 (2006).

[53] A. B. Ustinov and B. A. Kalinikos, A microwave nonlinear phase shifter, Appl. Phys. Lett. **93**, 102504 (2008).

[54] A. Sadovnikov, A. Grachev, V. Gubanov, S. Odintsov, A. Martyshkin, S. Sheshukova, Y. P. Sharaevskii, and S. Nikitov, Spin-wave intermodal coupling in the interconnection of magnonic units, Appl. Phys. Lett. **112**, 142402 (2018).

[55] A. Grachev, O. Matveev, M. Mruczkiewicz, M. Morozova, E. Beginin, S. Sheshukova, and A. Sadovnikov, Strain-mediated tunability of spin-wave spectra in the adjacent magnonic crystal stripes with piezoelectric layer, Appl. Phys. Lett. **118**, 262405 (2021).

[56] Q. Wang, T. Brächer, M. Fleischhauer, B. Hillebrands, and P. Pirro, Stimulated-Raman-adiabatic-passage mechanism in a magnonic environment, Appl. Phys. Lett. **118**, 182404 (2021).

[57] S. Watt and M. Kostylev, Reservoir Computing Using a Spin-Wave Delay-Line Active-Ring Resonator Based on Yttrium-Iron-Garnet Film, Phys. Rev. Appl. **13**, 034057 (2020).